

Decomposing the parameter space of biological networks via a numerical discriminant approach

Heather A. Harrington¹, Dhagash Mehta², Helen M. Byrne¹, and
Jonathan D. Hauenstein²

¹ Mathematical Institute, The University of Oxford, Oxford OX2 6GG, UK
`{harrington,helen.byrne}@maths.ox.ac.uk`,

`www.maths.ox.ac.uk/people/{heather.harrington,helen.byrne}`

² Department of Applied and Computational Mathematics and Statistics,
University of Notre Dame, Notre Dame IN 46556, USA
`{dmehta,hauenstein}@nd.edu`, `www.nd.edu/~{dmehta,jhauenst}`

Abstract. Many systems in biology (as well as other physical and engineering systems) can be described by systems of ordinary differential equation containing large numbers of parameters. When studying the dynamic behavior of these large, nonlinear systems, it is useful to identify and characterize the steady-state solutions as the model parameters vary, a technically challenging problem in a high-dimensional parameter landscape. Rather than simply determining the number and stability of steady-states at distinct points in parameter space, we decompose the parameter space into finitely many regions, the number and structure of the steady-state solutions being consistent within each distinct region. From a computational algebraic viewpoint, the boundary of these regions is contained in the discriminant locus. We develop global and local numerical algorithms for constructing the discriminant locus and classifying the parameter landscape. We showcase our numerical approaches by applying them to molecular and cell-network models.

Keywords: parameter landscape · numerical algebraic geometry · discriminant locus · cellular networks.

1 Introduction

The dynamic behavior of many biophysical systems can be mathematically modeled with systems of differential equations that describe how the state variables interact and evolve over time. The differential equations typically include parameters that represent physical processes such as kinetic rate constants, the strength of cell-cell interactions, and external stimuli. The qualitative behavior of the state variables may change as the parameters vary. Typically, determining and classifying all steady-state solutions of such nonlinear systems, as a function of the parameters, is a difficult problem. However, when the equations are polynomial, or can be translated into polynomials (e.g, rational functions), which is the case for many biological systems (as well as other physical and engineering

systems), computing the steady-state solutions becomes a problem in computational algebraic geometry. Thus, it is possible to compute the regions of the parameter space that give rise to different numbers of steady-state solutions.

1.1 Previous work

Due to the ubiquity of such problems, many methods have been proposed for identifying and characterizing steady-state solutions over a parameter space. A standard approach to understand changes in qualitative behavior of differential equations as a parameter is varied is to study bifurcations (singularities). Many standard bifurcation techniques focus on local behavior in the phase space near a structurally unstable object (e.g., fixed point) and the analysis is algebraic by focusing on the normal form [22, 20]. Numerical bifurcation techniques as implemented in, for example, AUTO [15] and MATCONT [14], require an initial starting point, use a root finding solver to find a fixed point, and then continue along a branch (e.g., via arc-length continuation). However, these methods are nearly all local in the phase space in that one “continues” (or “sweeps” [37]) from a given initial point. Thus, studying a larger phase space requires sampling of different initial conditions and parameter values. In recent years, computation of bifurcation diagrams of disconnected branches, so-called deflation continuation methods, have been developed [16], however, these do not guarantee finding all solutions at a particular parameter value.

We take a geometric approach and do not restrict ourselves to a local area of the phase space (e.g., no initial condition or guess) nor do we start our analysis by solving (e.g., using Newton’s method) for a single fixed point. We focus on where the discriminant vanishes – called the *discriminant locus* – in which roots merge along the discriminant as a parameter varied. Recall that when solving the equation $ax^2 + bx + c = 0$, where a , b , and c are parameters, and x is the variable, the discriminant locus defined by $\Delta := b^2 - 4ac = 0$ is the boundary separating regions in which the two distinct solutions for x are real ($\Delta > 0$) and nonreal ($\Delta < 0$). The discriminant locus, when arising from a system of ODEs, is often called the bifurcation variety [1]. A parametrization of the discriminant set (variety) can sometimes be computed explicitly, e.g., [8], but this is generally a difficult problem for systems with more than a handful of variables and parameters. Moreover, most of these methods, even those that can systematically ‘globally’ divide the parameter plane are local in the sense of the phase space [38]. Other symbolic methods are global in terms of phase space include using a cylindrical algebraic decomposition [12] with related variants [32, 46, 9] and computing the ideal of the discriminant locus using resultants or Gröbner basis methods, e.g., see [13, 18, 42, 34]. Unfortunately, each of these methods has potential drawbacks due to their algorithmic complexity, symbolic expression swell, and inherent sequential nature.

By using homotopy continuation and, more generally, numerical algebraic geometry (see [5, 39, 45]), all solutions over the complex numbers \mathbb{C} to a system of polynomial equations can be computed. In this sense, numerical algebraic geometry permits the computation, with probability one, of *all* real steady-state

solutions over a chosen region of parameter space effectively capturing the global behavior of the dynamical system and even detecting disconnected branches of solutions. Such methods have been implemented in software packages including Bertini [6], HOM4PS-3 [10], and PHCpack [43] with Paramtopy [3] extending Bertini to study the solutions at many points in parameter space. Typically, these methods work over \mathbb{C} while the solutions of interest in biological models are in a subset of the real numbers \mathbb{R} , e.g., one is interested in steady-states in the positive orthant where the variables are biologically meaningful.

1.2 Problem setup

The general framework of problems under consideration are autonomous systems of differential equations of the form

$$\frac{d}{dt}\mathbf{x} = \mathbf{f}(\mathbf{x}, \mathbf{p}) \quad (1)$$

where $\mathbf{x} = (x_1, \dots, x_N)$ denotes the state variables, $\mathbf{p} = (p_1, \dots, p_s)$ denotes the system parameters, and $\mathbf{f}(\mathbf{x}, \mathbf{p})$ is a system of N functions. For $\mathbf{p} \in \mathbb{R}^s$, since we aim to compute the *steady-state solutions* to Eq. 1, which are $\mathbf{x} \in \mathbb{R}^N$ such that $\mathbf{f}(\mathbf{x}, \mathbf{p}) = 0$. By using numerical algebraic geometry, we additionally require that $\mathbf{f}(\mathbf{x}, \mathbf{p}) = 0$ can be translated into solving polynomial equations, e.g., $\mathbf{f}(\mathbf{x}, \mathbf{p})$ consists of polynomial or rational functions. Moreover, we are particularly interested in the typical situation for biological networks where, for almost all \mathbf{p} , the system $\mathbf{f}(\mathbf{x}, \mathbf{p}) = 0$ has finitely many distinct (isolated) solutions, all of which are nonsingular, i.e., every eigenvalue of the Jacobian matrix $J_{\mathbf{x}}\mathbf{f}(\mathbf{x}, \mathbf{p})$ of \mathbf{f} with respect to the state variables is nonzero. Therefore, certified techniques are used to distinguish between real and nonreal solutions [29].

We consider the parameter space $\mathcal{P} \subset \mathbb{R}^s$ for Eq. 1 to consist of those parameter values \mathbf{p} that are biologically meaningful, e.g., \mathbb{R}^s or positive orthant in \mathbb{R}^s . The quantitative behavior of the steady-state solutions, that is, the number of them, not necessarily the value of the steady-state, is constant on subregions in \mathcal{P} , e.g., the number of physically realistic steady-state solutions is the same for all parameter values in a region. One can also refine the quantitative behavior, by restricting, for example, to only positive steady-state solutions that are locally stable. The points forming the boundaries of these regions are called *critical points* and collectively form the *discriminant locus*, which is called the *minimal discriminant variety* in [32]. The discriminant locus is contained in a hypersurface in \mathcal{P} .

Suppose that $\mathbf{p} \in \mathcal{P}$ is such that $\mathbf{f}(\mathbf{x}, \mathbf{p}) = 0$ is in the interior of a subregion in the complement of the discriminant locus. The implicit function theorem yields that the solutions can be extended to an open neighborhood containing \mathbf{p} . One can keep increasing the size of this neighborhood in the parameter space until it touches the discriminant locus.

1.3 Contribution and organization of paper

In Section 2, we present a *numerical discriminant locus* method for decomposing the parameter space into distinct solution regions effectively stratifying the pa-

Algorithm 1: Perturbed sweeping

Input: Parameterized equations $\mathbf{f}(\mathbf{x}, p) = 0$ which can be translated into solving polynomial equations with parameter space $\mathcal{P} \subset \mathbb{R}$, perturbation $\epsilon \in \mathbb{R} \setminus \{0\}$, and description of the discriminant Δ associated with quantitative behavior of interest.

Output: Description of the intervals in the parameter space \mathcal{P} with the same quantitative behavior.

Randomly select $p^* \in \mathcal{P}$ and compute the solution set $S \subset \mathbb{C}^N$ of $\mathbf{f}(\mathbf{x}, p^* + \epsilon\sqrt{-1}) = 0$. Track each smooth solution path parameterized by $p \in \mathcal{P}$ defined by $\mathbf{f}(\mathbf{x}, p + \epsilon\sqrt{-1}) = 0$ with start points S at $p = p^*$.

Use the solution paths to approximate all values of $p \in \mathcal{P}$ where a solution path becomes ill-conditioned and refine, e.g., using [21, 23], to identify the critical points $C \subset \mathcal{P}$ where the quantitative behavior of interest changes.

Return the set of intervals of \mathcal{P} whose endpoints are consecutive points in C .

parameter space. We propose three methods for decomposing the parameter space that build upon advances in real numerical algebraic geometry. A schematic is given in Figure 1. The first (Alg. 1) is for one-dimensional parameter spaces in which case the discriminant locus consists of finitely many points. We enhance sweeping approaches such as [27, 37] with a perturbation and use all solutions simultaneously to locate the finitely many regions, which are open intervals in this case, where the number of steady-state solutions is consistent. The second (Alg. 2) is for low-dimensional parameter spaces and provides a complete decomposition of the parameter space into finitely many regions after decomposing the discriminant locus. Since computing and decomposing the discriminant locus may be impractical for high-dimensional parameter spaces, our third method (Alg. 3) uses the sweeping approach to compute a local decomposition of the parameter space near a given point in the parameter space. When decomposing a high-dimensional parameter space is desirable, one could bootstrap together local analyses to generate a more complete, or global, view of the parameter space.

In Section 3, we apply these algorithms to two biological models. The first is a detailed ODE model involving rational functions of gene and protein signaling network that induces long-term memory proposed in [36]. We demonstrate our method goes beyond singularity theory results in [40]. The second is a new network model of cell fate specification in a population of interacting stem cells where the algorithms provide insight into the qualitative behaviors that the model can exhibit.

The paper concludes in Section 4.

2 Decomposition using numerical algebraic geometry

This section reviews the required ingredients from numerical algebraic geometry with expanded details provided in, e.g., [5, 39, 45]. Traditionally, symbolic approaches such as [12, 32] describe the regions using both equations that vanish on the discriminant locus and inequalities, e.g., see [35, 26, 31, 24] for applications to biology. The key observation from numerical algebraic geometry is to replace computing equations and inequalities with geometric descriptions as described below. We can use numerical algebraic geometry techniques presented in

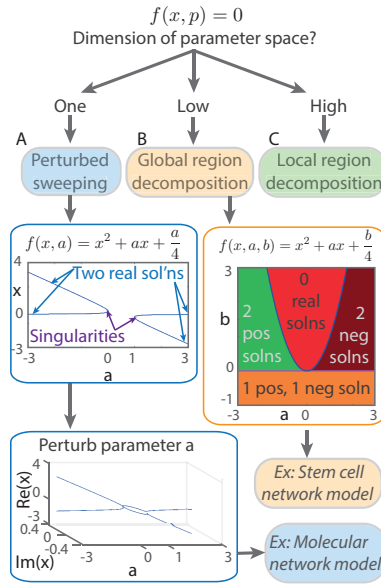


Fig. 1. Flow chart of methods. **(A)** Perturbed sweeping. **(B)** Global method for decomposing (a, b) parameter space into regions based on number of real steady-states. **(C)** Local method for high dimensional parameter space analysis.

Algorithm 2: Global decomposition of 2-dimensional parameter space

Input: Parameterized equations $\mathbf{f}(\mathbf{x}, \mathbf{p}) = 0$ which can be translated into solving polynomial equations, parameter space $\mathcal{P} \subset \mathbb{R}^2$, and description of the discriminant Δ associated with quantitative behavior of interest.

Output: Description of regions in the parameter space \mathcal{P} with the same quantitative behavior.

Randomly select $\alpha \in \mathbb{R}^2$ and $\mu^* \in \mathbb{R}$, and compute the simultaneous solution set $S \subset \mathbb{C}^N \times \mathbb{C}^2$ of $\mathbf{f}(\mathbf{x}, \mathbf{p}) = 0$, $\alpha \cdot \mathbf{p} = \mu^*$, and the discriminant locus $\Delta = 0$.

Use isosingular deflation [30] as needed to permit tracking on the discriminant locus intersected with the line $\alpha \cdot \mathbf{p} = \mu$ parameterized by μ .

Apply perturbed sweeping where $\mu \in \mathbb{R}$ is the parameter to compute the critical points $C \subset \mathbb{R}$ of the discriminant locus intersected with the line $\alpha \cdot \mathbf{p} = \mu$.

If \mathcal{P} has a boundary, append to C the values of $\alpha \cdot \mathbf{p}$ such that \mathbf{p} lies at the intersection of the discriminant locus and the boundary of \mathcal{P} .

Between two consecutive values in C , say $\mu_1 < \mu_2$, pick $\mu = (\mu_1 + \mu_2)/2$ and use perturbed sweeping to compute a decomposition into intervals along the line $\alpha \cdot \mathbf{p} = \mu$ inside of \mathcal{P} . Connect the boundaries of these intervals to the endpoints μ_1 and μ_2 to create a region decomposition between critical points. Optionally, merge regions across slices $\alpha \cdot \mathbf{p} = \mu_j$ for $j = 1, 2$ which have the same quantitative behavior.

Return the regions of \mathcal{P} .

Section 2.4 to compute every point in the intersection of a line with the discriminant locus and then compute the boundary of the region. Finding sample points in the interior of the regions (which is not on the discriminant locus) has been suggested, e.g., [34, 33, 2, 7]. *Isosingular deflation* developed in [30] allows one to construct a system for tracking along the discriminant locus thereby tracing out the corresponding boundary. Adaptive multiprecision path tracking [4] is used to

Algorithm 3: Local decomposition of parameter space

Input: Parameterized equations $\mathbf{f}(\mathbf{x}, \mathbf{p}) = 0$ which can be translated into solving polynomial equations, parameter space $\mathcal{P} \subset \mathbb{R}^s$, description of the discriminant Δ associated with quantitative behavior of interest, and point $\mathbf{p}^* \in \mathcal{P}$ that is not contained in the discriminant locus.

Output: Description of some regions of the parameter space \mathcal{P} with the same quantitative behavior.

Randomly select a direction $\boldsymbol{\alpha}^* \in \mathbb{R}^s$ and apply perturbed sweeping to the system $\mathbf{f}(\mathbf{x}, \mathbf{p}^* + \mu\boldsymbol{\alpha}^*) = 0$ parameterized by μ .

Use isosingular deflation [30] as needed to permit tracking on the discriminant locus intersected with the linear space parameterized by $\mathbf{p}^* + \mu\boldsymbol{\alpha}$ as $\boldsymbol{\alpha}$ varies.

Apply path tracking to vary $\boldsymbol{\alpha}$ to trace out boundaries of regions inside of \mathcal{P} with the same quantitative behavior.

Return the regions of \mathcal{P} whose boundaries were traced out.

ensure reliable numerical computations, especially near the discriminant locus. The computations described in Section 3 adaptively changed between double, 64-bit, and 96-bit precision.

2.1 Computing all solutions

From algebraic geometry, a parameterized system of equations $\mathbf{f}(\mathbf{x}, \mathbf{p}) = 0$ which are polynomial or can be translated into polynomials has a *generic* behavior for parameters \mathbf{p} over the complex numbers. For example, the number of distinct solutions of $\mathbf{f}(\mathbf{x}, \mathbf{p}) = 0$ for almost all $\mathbf{p} \in \mathbb{C}^s$ are equal. Therefore, a random choice of $\mathbf{p} \in \mathbb{C}^s$, say \mathbf{p}^* , will have the generic behavior *with probability one*. Classical homotopy continuation, e.g., see [5, 39], permits one to compute all distinct solutions of $\mathbf{f}(\mathbf{x}, \mathbf{p}^*) = 0$. One can then continue the solutions of $\mathbf{f}(\mathbf{x}, \mathbf{p}^*) = 0$ via a *parameter homotopy* to solve $\mathbf{f}(\mathbf{x}, \mathbf{p}) = 0$ for any other parameter value \mathbf{p} . This improves computational efficiency since solving at other parameter values is typically much faster than the *ab initio* solving of $\mathbf{f}(\mathbf{x}, \mathbf{p}^*) = 0$.

2.2 Perturbed sweeping

For one-dimensional parameter spaces, i.e., $s = 1$, the discriminant locus consists of at most finitely many points. Thus, the parameter p parameterizes solution paths $\mathbf{x}(p)$ defined by $\mathbf{f}(\mathbf{x}(p), p) = 0$ which can be tracked. In particular, one can *sweep* [27, 37] as p varies and locate all values of p where a solution path is not smooth, i.e., where $J_{\mathbf{x}}\mathbf{f}(\mathbf{x}(p), p)$ has a zero eigenvalue. Since each solution path $\mathbf{x}(p)$ satisfies

$$\frac{d\mathbf{x}}{dp} = -J_{\mathbf{x}}\mathbf{f}(\mathbf{x}, p)^{-1} \cdot J_p\mathbf{f}(\mathbf{x}, p), \quad (2)$$

numerical ill-conditioning will occur near the discriminant locus. In fact, Eq. 2 will become stiff since $J_{\mathbf{x}}\mathbf{f}(\mathbf{x}, p)$ is not invertible on the discriminant locus.

Rather than attempting to track through the discriminant locus, we propose a *perturbed sweeping* approach that guarantees smoothness of the path for easier tracking while still observing some ill-conditioning for identifying the discriminant locus. An example of this is shown in Figure 2 in Section 2.5.

Theorem 1. *For $i = \sqrt{-1}$ and $\epsilon \in \mathbb{R}$, we consider the perturbed solution paths $\mathbf{x}_\epsilon(p)$ defined by $\mathbf{f}(\mathbf{x}_\epsilon(p), p + \epsilon i) = 0$. With the setup described above, for all but finitely many $\epsilon \in \mathbb{R}$, all perturbed solution curves are smooth.*

Proof. Since there are only finitely many points in the discriminant locus over the complex numbers, there can be only finitely many values of $\epsilon \in \mathbb{R}$ such that there exists $\delta \in \mathbb{R}$ with $\delta + \epsilon i$ in the discriminant locus.

Since $\mathbf{x}_\epsilon(p) \rightarrow \mathbf{x}(p)$ as $\epsilon \rightarrow 0$, we can recover information about the actual solution curves by monitoring the condition number as in [27] with the distinct numerical advantage of tracking *smooth* solution curves. If further refinement is needed, additional efficient local computations can be employed, e.g., [21, 23].

2.3 Global region decomposition

We now build upon the perturbed sweeping approach to decompose parameter spaces which are not one-dimensional. This approach, called a *global region decomposition*, is applicable for low-dimensional parameter spaces which mixes projections, critical sets, and perturbed sweeping. For illustration, we start in the two-dimensional case, i.e., $s = 2$, for which the discriminant locus is contained in a curve. Given $\boldsymbol{\alpha} \in \mathbb{R}^2$ and $\mu \in \mathbb{R}$, we consider intersecting the discriminant locus with the line $\pi_{\boldsymbol{\alpha}}(\mathbf{p}) := \boldsymbol{\alpha} \cdot \mathbf{p} = \mu$. For almost all choices of $(\boldsymbol{\alpha}, \mu) \in \mathbb{R}^2 \times \mathbb{R}$, i.e., with probability one for randomly selected $(\boldsymbol{\alpha}, \mu) \in \mathbb{R}^2 \times \mathbb{R}$, there are at most finitely many values of \mathbf{p} such that the line $\pi_{\boldsymbol{\alpha}}(\mathbf{p}) = \mu$ intersects the discriminant locus. Hence, we can use the perturbed sweeping approach along this line to compute these values. For example, an initial plot of the global region decomposition can be made by simply selecting various values of $\boldsymbol{\alpha}$ and μ and plotting the various regions along the various lines $\pi_{\boldsymbol{\alpha}}(\mathbf{p}) = \mu$.

To create a complete global region decomposition, we follow a modification of [33]. First, we compute all $\mathbf{p} \in \mathbb{C}^2$ such that the line defined by $\pi_{\boldsymbol{\alpha}}(\mathbf{p}) = \mu$ intersects the discriminant locus via homotopy continuation. We solve in \mathbb{C}^2 here since the number of real intersection points need not be constant whereas the complex numbers ensures that we will locate every real component. One then uses isosingular deflation [30] as needed to construct a system which permits the tracking along the discriminant locus intersected with the line $\pi_{\boldsymbol{\alpha}}(\mathbf{p}) = \mu$. Perturbed sweeping viewing μ as a parameter moves the line in parallel sweeping out the entire plane yielding critical points of the discriminant locus with respect to μ . Hence, if $\mu_1 < \mu_2$ are two consecutive critical points, we know that the topology of the global region decomposition along the line $\pi_{\boldsymbol{\alpha}}(\mathbf{p}) = \mu$ for $\mu \in (\mu_1, \mu_2)$ is equivalent, e.g., same number of intervals which connect up to form regions. Hence, one simply connects the regions across the critical points to form the global regions. An example of this is presented below in Section 2.5.

For higher-dimensional spaces, a global region decomposition is computed by applying global region decomposition to smaller-dimensional spaces. For example, one can compute a global region decomposition on a plane inside of a high-dimensional parameter space using the two-dimensional method described

above. By selecting various planes, one obtains an initial plot of the global region decomposition. To have a complete picture, one can utilize projections into lower-dimensional spaces computing critical sets of the discriminant locus to locate all areas where the quantitative behavior can change. For example, in the three-dimensional case, $s = 3$, with linear map $\pi_{\alpha,\beta}(\mathbf{p}) = (\alpha \cdot \mathbf{p}, \beta \cdot \mathbf{p})$ where $\alpha, \beta \in \mathbb{R}^3$, one first considers the parameter space of $\mu \in \mathbb{R}^2$ where $\pi_{\alpha,\beta}(\mathbf{p}) = \mu$. By computing a global region decomposition for $\mu \in \mathbb{R}^2$ with respect to the critical curve of the original discriminant locus, one can then stitch together a global region decomposition in the original three-dimensional space as follows. Upon fixing $\mu \in \mathbb{R}^2$ inside of a region, one obtains a curve in the original three-dimensional parameter space where the finitely many points on the discriminant locus can be found using perturbed sweeping. Then, applying isosingular deflation [30] as needed permits the tracking of the original discriminant locus as one moves $\mu \in \mathbb{R}^2$ inside of its corresponding region to connect neighboring regions at the critical points.

2.4 Local region decomposition

Since a global region decomposition is not practical for high-dimensional parameter spaces, we propose a local region decomposition method by combining perturbed sweeping with the classical approach of ray tracing, e.g., see [19]. Given a point $\mathbf{p} \in \mathcal{P}$ not contained in the discriminant locus, which happens for a random point with probability one, the codimension-one components of the discriminant locus can be obtained by using the perturbed sweeping approach along lines emanating from \mathbf{p} , say in the direction α , yielding the real values of μ for which the corresponding line parameterized by $\mathbf{p} + \mu\alpha$ intersects the discriminant locus. As above, once points on the discriminant locus are found, applying isosingular deflation [30] as needed permits the tracking along the discriminant locus tracing the region boundaries as one changes α .

This method is local in the sense that one is only tracing along the real points obtained by the intersection of the codimension one components of the discriminant locus with the line parameterized by $\mathbf{p} + \mu\alpha$. As mentioned in Section 2.3, the number of such real points can change as one changes α . To overcome this, one could first compute all such complex intersection points and track all of the corresponding paths as one changes α . Thus, one can be sure to obtain all real points of intersection along any other direction emanating from \mathbf{p} . Even though lower-dimensional boundaries of the regions could be missed with such an approach, it avoids the expense of computing critical points of projections. Nonetheless, local decompositions starting from various \mathbf{p} with various α can provide a reasonable plot of the main features of a global decomposition of the parameter space.

2.5 Quadratic example

To illustrate the perturbed sweeping and global region decomposition approach, we consider two examples of a parameterized quadratic equation. The first has one parameter, namely $f(x, a) = x^2 + ax + a/4$. The classical discriminant for

quadratic polynomials yields $\Delta = a^2 - a$ with discriminant locus $\{0, 1\}$. In particular, $f = 0$ has two distinct real solutions when $a < 0$ or $a > 1$, two distinct complex (i.e., nonreal) solutions when $0 < a < 1$, and a multiplicity 2 real solution when $a = 0$ or $a = 1$. The perturbed sweeping method avoids tracking through the the singularities to have two smooth paths $x_\epsilon(a)$ defined by $f(x_\epsilon(a), a + \epsilon i) = 0$ for any $\epsilon \in \mathbb{R} \setminus \{0\}$ and $a \in \mathbb{R}$. For example, with $\epsilon = 10^{-6}$, we sweep along the smooth $x_\epsilon(a)$ and observe the expected solution behavior as shown in Figure 1A where the number of real solutions changes at the singularities $a = 0$ and $a = 1$, which are clearly observed in Figure 2.

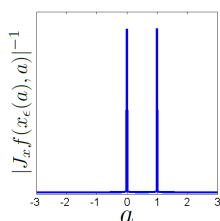


Fig. 2. Illustration of using perturbed sweeping to locate singularities at $a = 0, 1$.

The second example is $f(x, a, b) = x^2 + ax + b/4$ which has two parameters and is shown in Figure 1B. We aim to decompose the parameter space where the quantitative behavior of interest is the number of real and positive solutions, which is typical in biological problems. The discriminant locus for this situation corresponds with the closure of (a, b) such that there exists x such that $f(x, a, b) = 0$ and $x(2x + a) = 0$. In particular, the corresponding discriminant locus consists of two irreducible curves, defined by $b = 0$ and $a^2 = b$, which cut the parameter space $(a, b) \in \mathbb{R}^2$ into four regions where the number of real, positive, and negative solutions are constant on these regions as shown in Figure 1B. The following describes the essence of computing a global region decomposition.

Consider taking $\alpha = (1, 0)$ so that $\pi_\alpha(a, b) = a$. Fixing, say, $\mu^* = 0.5$, we use perturbed sweeping along the line defined by $\pi_\alpha(a, b) = a = \mu^* = 0.5$. This locates the two real points on the discriminant locus, namely $b = 0$ and $b = 0.25$. we do not need to apply isosingular deflation since both are nonsingular solutions with respect to the discriminant system $f(x, a, b) = 0$ and $x(2x + a) = 0$.

Next, we use perturbed sweeping with these two solutions parameterized by μ starting at $\mu^* = 0.5$ to locate critical points of the discriminant locus. This locates the critical point of the discriminant locus when $\pi_\alpha(a, b) = a = \mu = 0$.

Finally, we simply need to put everything together. At the critical point of the discriminant locus at $a = 0$, there are two regions in terms of b , namely $b < 0$ and $b > 0$. For any $a < 0$ or $a > 0$, there are three regions in terms of b , namely $b < 0$, $0 < b < a^2$, and $b > a^2$. Hence, can merge together the regions $b < 0$ and $b > a^2$ for $a < 0$ and $a > 0$ at the critical point $a = 0$. Therefore, this yields a global region decomposition consisting of 4 distinct regions shown in Figure 1B.

3 Results from biological models

We showcase our methods by applying them to two biological models. First, we analyze a detailed ODE model of the gene and protein signaling network that induces long-term memory proposed by Pettigrew *et al.* [36]. We demonstrate that our method can be applied to rational functions and reproduce known bifurcation results. Moreover, we find an additional, disconnected branch solution using our method. The second model is a network of cell fate specification in a population of interacting stem cells with complicated dynamics. Since cellular decision making often depends on the number of accessible (stable) steady-states that a system exhibits, we seek to identify distinct regions of parameter space that can elicit different system behavior.

3.1 Molecular network model

A gene and protein network for long-term memory was proposed by Pettigrew *et al.* [36] and investigated using bifurcation and singularity analysis by Song *et al.* [40]. The model is of the form of Eq. 1 where \mathbf{f} consists of 15 rational functions, $\mathbf{x} \in \mathbb{R}^{15}$ is the vector of model variables, and $\mathbf{p} \in \mathbb{R}^{40}$ is the vector of parameters. The following summarizes the structure of the 15 rational functions:

numerator degree	denominator degree	number of functions in \mathbf{f}
1	0	2
2	0	2
2	1	1
3	1	4
3	2	2
4	2	3
5	4	1

For a random choice of parameters \mathbf{p} , the system of equations $\mathbf{f}(\mathbf{x}, \mathbf{p}) = 0$ has 432 isolated nonsingular solutions.

We demonstrate that our discriminant method can 1) reproduce their results as a proof-of-principle, 2) handle rational functions, and 3) we find an additional solution branch not previously located. For this system, the denominators do not vanish near the regions of interest so they do not have any impact on the behavior of the solutions. If the denominator also vanished when finding a solution to the system of equations from the numerators, then the parameter values for which this occurs would be added into the discriminant locus.

We fix the model parameters using the values from [40]. This leaves two parameters to investigate, namely λ which represents the extracellular stimulus [5-HT] and k_{ApSyn} . The variable of biological interest required for long-term facilitation is the steady-state of protein kinase A (PKA) in response to the extracellular stimulus parameter λ . Our aim is to demonstrate the perturbed sweeping method on a large model to reproduce results from Figure 5 of [40]. In particular, we verify all of their solution branches but also find another solution not reported, which is the top branch shown in Figure 3. This demonstrates the power of this method to ensure all real solutions are computed. On inspection, this additional steady-state is not on the same branch, but is not biologically feasible so we can reject it as nonphysical. However, by using such an exhaustive first step, we can identify all steady-states, and then systematically characterize and check each solution.

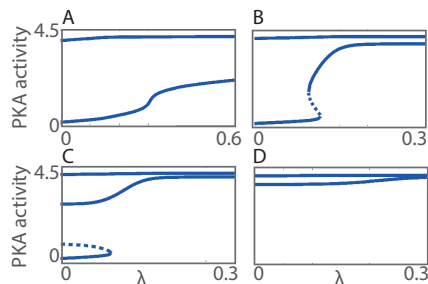


Fig. 3. Results of perturbed sweeping method applied to molecular network model of long-term memory that plots the behavior of protein kinase A (PKA) in response to changes in λ , which is the extracellular stimulus [5-HT], for elected values of k_{ApSyn} as in [40, Fig. 5]. Solid lines denote a stable steady-state while dashed lines denote an unstable steady-state. (A) Parameter $k_{\text{ApSyn}} = 0.0022$. (B) Parameter $k_{\text{ApSyn}} = 0.015$. (C) Parameter $k_{\text{ApSyn}} = 0.03$. (D) Parameter $k_{\text{ApSyn}} = 0.1$.

3.2 Cellular network model

Most multicellular organisms emerge from a small number of stem-like cells which become increasingly specialized as they proliferate until they transition to one of a finite number of differentiated states [11]. We propose a caricature model of cell fate specification for a ring of cells, and investigate how cell-cell interactions, mediated by diffusive exchange of a key growth factor, may affect the number of (stable) configurations or patterns that the differentiated cells may adopt. The model serves as a good test case for these discriminant locus methods since, by construction, there is an upper bound on the number of feasible steady-states (2^N stable solutions for a ring of N cells) and some of these patterns are equivalent due to symmetries inherent in the governing equations.

We consider a ring of N interacting cells and denote by $x_i(t) \geq 0$ the concentration within cell i of a growth factor or protein (e.g., notch), whose value determines that cell's differentiation status [17, 41, 47, 44, 25]. For $0 < \varepsilon < a < 1$, the subcellular dynamics of x_i are represented by a phenomenological function $q(x_i) = (x - \varepsilon)(x - a)(1 - x)$. This function guarantees bistability of each cell in the absence of cell-cell communication. The bistability represents two distinct cell fates, e.g., high and low levels of notch, which may be associated with differentiation of intestinal epithelial cells into secretory and absorptive phenotypes [17, 41, 11]. We assume further that cell i communicates with its nearest neighbors (cells $i \pm 1$) via diffusive exchange of x_i and denote by a parameter $g \geq 0$ that describes the coupling strength. Thus, our cell-network model is

$$\frac{dx_i}{dt} = q(x_i) + g \cdot \sum_{j=i-1}^{i+1} (x_j - x_i), \text{ for all } i = 1, \dots, N. \quad (3)$$

This model assumes uniform coupling g for all nearest neighbors as well as periodic boundary conditions ($x_{N+1} \equiv x_1$ and $x_0 \equiv x_N$), as shown in Figure 4A.

We analyze the model by using the global region decomposition method for $N = 3, 4, 5$ cells and construct classification diagrams in (a, g) parameter space (Figure 4B). In addition to decomposing the parameter space into regions based on the number of steady-state solutions, the method also provides valuable information about how solution structure and stability changes as the system parameters vary. For example, in Figure 4C for the $N = 3$ cell-network, we show how the values and stability of the steady-states for (x_1, x_2, x_3) change as a varies with $g = 0.025$ and as g varies with $a = 0.4$ where $\varepsilon = 0.01$. In Figure 4D, we plot bifurcation diagrams as a and g vary as before for the $N = 4$ cell-network. In this plot, instead of presenting particular components x_i ($i = 1, 2, 3, 4$), we plot the 2-norm ($\|\mathbf{x}\|_2 = (x_1^2 + x_2^2 + x_3^2 + x_4^2)^{1/2}$) to capture the multiplicity of solutions. We note that for $N = 3$ and $N = 4$ there are always two stable and one unstable steady-states, independent of (a, g) parameter values (as shown by the black and red points in Figure 4C, and by the solid blue lines in Fig. 4D).

For $N = 4$, the classical discriminant locus for this model can be shown to have degree 72 using homotopy continuation. That is, there is a degree 72 polynomial $\Delta(a, g)$ such that the classical discriminant locus is defined by $\Delta = 0$. Even though we were unable to compute this polynomial explicitly, the advantage of using numerical algebraic geometry, as first described in [28], is that computations can be performed on this discriminant locus without having explicit defining equations. In particular, with $a = 0.4$ as in Figure 4D, the univariate polynomial equation $\Delta(0.4, g) = 0$ has 45 complex solutions, 25 of which are real. Of these 25 real solutions, 15 are positive with only 4 of them corresponding to where change in the number of stable steady-state solutions occur. The regions (intervals) for $g \geq 0$ when $a = 0.4$ are approximately:

region	# stable steady-state soins
$[0, 0.0197)$	16
$(0.0197, 0.0206)$	12
$(0.0206, 0.0411)$	10
$(0.0411, 0.0533)$	6
$(0.0533, \infty)$	2

We now interpret the results in the context of cell-cell communication. We notice that intermediate values of a generate the largest number of real stable steady-states; small and high values of a yield fewer real stable steady-states. Interestingly, all cells synchronize for intermediate to strong values of the coupling parameter g (two stable states in blue region in Figure 4B). We conclude that strong cell-cell communication reduces the number of stable steady-state configurations that a population of cells can adopt and, thus, cell-cell communication could be used robustly to drive the cells to a small number of specific states. When coupling is weak ($0 < g < 0.1$), the interacting cells have more flexibility in terms of their final states, with the 5-cell network admitting up to 32 stable steady-states (Figure 4B(iii)). Weaker cell-cell communication allows more patterns to emerge and may be appropriate when it is less important that neighboring cells share the same phenotype. We find that the regions of (a, g) parameter space that give rise to more than two (synchronized) steady-states also increase in size as the number of cells increases.

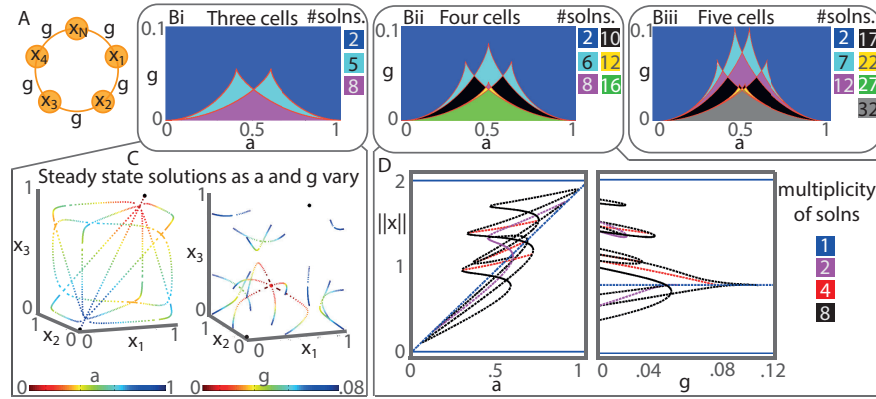


Fig. 4. Global region decomposition applied to coupled cell-network model. **(A)** Ring of cell-network. Each cell x_i has bistable dynamics at stable states at 0 and 1, and unstable state given by a . The cells are coupled to neighbour cells by a coupling strength parameter g . **(B)** Region decomposition with parameters a, g , similar to a classification diagram, with the number of real stable steady-stages denoted by different colors. The number of stable real steady-states is given for each network where $N = 3, 4$, and 5 . **(C)** Steady-state values in state space for $N = 3$ cell-network are plotted as parameter a is varied between $[\varepsilon, 1]$ or g is varied. The two black dots are stable steady-states, the red is an unstable steady-state, these steady-states are independent of parameter values a and g . **(D)** Bifurcation diagram showing $\|x\|_2$ as the parameters are varied.

3.3 Chain of cells

We next consider a chain of cells rather than a ring. We demonstrate the ability of the local region decomposition method to analyze a generalization of Eq. 3 in which the coupling strength between two cells is not constant. For this caricature stem-cell model, we have classified the number of stable steady-states as the cell-cell coupling parameters are varied, and this increases the dimension of the parameter space. Visualization of the decomposition of higher dimensional parameter spaces is difficult, therefore we created a movie which we describe below. This movie along with code dependent on Bertini [6] and MATLAB used to generate it is available at the repository <http://dx.doi.org/10.7274/R0P848V0>.

To that end, we consider a generalization of the model given in Eq. 3 which uses coupling strengths $g_{i,i+1} = g_{i+1,i} \geq 0$ between cell i and $i + 1$ with cyclic ordering ($N + 1 \equiv 1$), namely

$$\frac{dx_i}{dt} = q(x_i) + \sum_{j=i-1}^{i+1} g_{i,j} \cdot (x_j - x_i), \text{ for all } i = 1, \dots, N. \quad (4)$$

With $N = 4$, the classical discriminant locus for this generalized model has degree 486. We consider the case with $\varepsilon = 0.01$, $a = 0.4$, and $g_{4,1} = g_{1,4} = 0$ leaving three free parameters: $g_{1,2}$, $g_{2,3}$, and $g_{3,4}$.

First, we consider the perturbed sweeping approach along the ray defined by $g_{i,i+1} = i \cdot \mu$ for $i = 1, 2, 3$ and $\mu \geq 0$. This decomposes the space $\mu \geq 0$ into 15 regions, approximately

regions	# stable steady-state soins
(0, 0.0079)	16
(0.0079, 0.0080)	15
(0.0080, 0.0132)	14
(0.0132, 0.0136)	13
(0.0136, 0.0137)	12
(0.0137, 0.0142)	11
(0.0142, 0.0153)	10
(0.0153, 0.0161)	9
(0.0161, 0.0171)	8
(0.0171, 0.0237)	7
(0.0237, 0.0352)	6
(0.0352, 0.0360)	5
(0.0360, 0.0407)	4
(0.0407, 0.1264)	3
(0.1264, ∞)	2

As a comparison, the classical discriminant with respect to $\mu \in \mathbb{C}$ consists of 312 distinct points of which 84 are real. Of these, 42 are positive with 14 corresponding to a change in the number stable steady-state solutions.

Next, we vary $g_{1,2}$ and $g_{3,4}$ for a fixed $g_{2,3}$ (see Figure 5). As this is a chain of cells, we observe a natural symmetry as $g_{1,2}$ and $g_{3,4}$ vary for fixed values of $g_{2,3}$. Additionally, as the strength of the cell-cell coupling is increased, the number of stable steady-states decreases monotonically from a maximum value of 16 when coupling is weak down to the minimum value of 2 when coupling is strong where the rate of decline depending on the choice of parameter values.

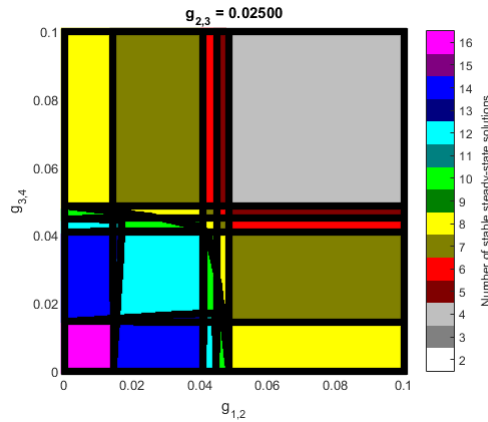


Fig. 5. Frame showing how, when $N = 4$ and $g_{2,3} = 0.025$, the number of stable steady-state solutions for Eq. 4 changes as $g_{1,2}$ and $g_{3,4}$ vary.

Finally, we determine how the how the number of stable steady-state solutions change as we move through the three-dimensional parameter using a movie. Each frame of the movie is based on a fixed value of $g_{1,2}$ and shows the decomposition of the plane involving $g_{2,3}$ and $g_{3,4}$. Figure 6 contains four frames from this movie. In particular, as the coupling $g_{1,2}$ increases, the maximum number

of stable steady-states decreases (from 16 when $g_{1,2} = 0$ to 8 when $g_{1,2} = 0.1$). We note that when $g_{1,2} > 0$, the frames in the parameter space $(g_{2,3}, g_{3,4})$ are no longer symmetric. We note also the appearance of regions of parameter space in which, for fixed values of $g_{1,2}$, the number of stable steady-states no longer decreases monotonically with $g_{2,3}$ or $g_{3,4}$. These results, which would not easily be accessible using standard analytical tools, highlight the rich structure of the cell-network model and the power of the local region decomposition method for identifying these solutions.

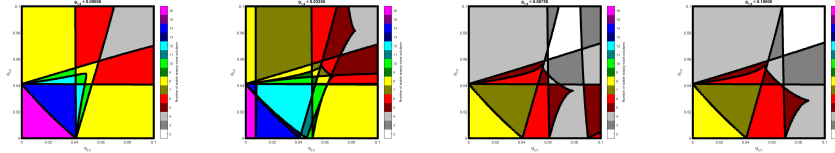


Fig. 6. Series of frames showing how, for fixed values of the parameter $g_{1,2} = 0.0, 0.0325, 0.0675, 0.1$ and $N = 4$, the number of stable steady-state solutions for Eq. 4 changes as $g_{2,3}$ and $g_{3,4}$ are varied.

4 Conclusion

We have presented a suite of numerical algebraic geometric methods for decomposing the parameter space associated with a dynamical system into distinct regions based on the multiplicity and stability of its steady-state solutions. The methods enable us to understand the parameter landscape of high-dimensional, ordinary differential models with large numbers of parameters. These methods have considerable potential: they could be used to analyze differential equation models associated with a wide range of real-world problems in biology, science, and engineering which cannot easily be tackled with existing approaches.

We have demonstrated that coupling the dynamics of cells, which individually exhibit bistable internal dynamics, can increase markedly the number of real stable steady-states that population exhibits. We considered different network topologies (rings and chains of cells) as well as heterogeneity of cell-cell coupling strengths using the local region decomposition. This methodology may help us to understand how stem cells within the intestinal crypt are able to generate differentiated cells with an array of absorptive and secretory phenotypes, just by considering the interaction of the cells as a network.

Acknowledgement

We thank J. Byrne and G. Moroz for helpful discussions. JDH was supported in part by NSF ACI 1460032 and CCF 1812746, Sloan Research Fellowship, and

Army Young Investigator Program (YIP). HAH acknowledges funding from EPSRC Fellowship EP/K041096/1, Royal Society University Research Fellowship, and AMS Simons Travel Grant.

References

1. Arnol'd, V.I., Goryunov, V.V., Lyashko, O.V., Vasil'ev, V.A.: Singularity Theory II Classification and Applications. In *Dynamical Systems VIII. Encyclopaedia of Mathematical Sciences*, vol 39. Springer, Berlin, Heidelberg (1993).
2. Bates, D.J., Brake, D.A., Hauenstein, J.D., Sommese, A.J., Wampler, C.W.: On computing a cell decomposition of a real surface containing infinitely many singularities. In: *Mathematical software—ICMS 2014, Lecture Notes in Comput. Sci.*, vol. 8592, pp. 246–252. Springer, Heidelberg (2014).
3. Bates, D.J., Brake, D.A., Niemerg, M.E.: Paramotopy: Parameter homotopies in parallel. Available at paramotopy.com (2015).
4. Bates, D.J., Hauenstein, J.D., Sommese, A.J., Wampler, C.W.: Adaptive multi-precision pathtracking. *SIAM J. Numer. Anal.* **46**(2), 722–746 (2008).
5. Bates, D.J., Hauenstein, J.D., Sommese, A.J., Wampler, C.W.: Numerically solving polynomial systems with Bertini, vol. 25. SIAM (2013).
6. Bates, D.J., Hauenstein, J.D., Sommese, A.J., Wampler II, C.W.: Software for numerical algebraic geometry: a paradigm and progress towards its implementation. In: *Software for algebraic geometry*, pp. 1–14. Springer (2008).
7. Besana, G.M., Di Rocco, S., Hauenstein, J.D., Sommese, A.J., Wampler, C.W.: Cell decomposition of almost smooth real algebraic surfaces. *Numer. Algorithms* **63**(4), 645–678 (2013).
8. Broer, H.W., Golubitsky, M., Vegter, G.: The geometry of resonance tongues: a singularity theory approach. *Nonlinearity*, **16**(4), 1511–1538 (2003).
9. Brown, C.W.: Qepcad b: a program for computing with semi-algebraic sets using cads. *ACM SIGSAM Bulletin* **37**(4), 97–108 (2003).
10. Chen, T., Lee, T.L., Li, T.Y.: Hom4PS-3: a parallel numerical solver for systems of polynomial equations based on polyhedral homotopy continuation methods. In: *Mathematical software—ICMS 2014, Lecture Notes in Comput. Sci.*, vol. 8592, pp. 183–190. Springer, Heidelberg (2014).
11. Clevers, H.: STEM CELLS. What is an adult stem cell? *Science* **350**(6266), 1319–1320 (2015).
12. Collins, G.E.: Quantifier elimination for real closed fields by cylindrical algebraic decomposition. In: *Automata theory and formal languages (Second GI Conf., Kaiserslautern, 1975)*, pp. 134–183. *Lecture Notes in Comput. Sci.*, Vol. 33. Springer, Berlin (1975).
13. Cox, D.A., Little, J., O'Shea, D.: *Using algebraic geometry*, Graduate Texts in Mathematics, vol. 185. Springer, New York, second edn. (2005).
14. Dhooge, A., Govaerts, W., Kuznetsov, Y.A.: Matcont: a matlab package for numerical bifurcation analysis of odes. *ACM Transactions on Mathematical Software (TOMS)* **29**(2), 141–164 (2003).
15. Doedel, E.J.: Auto: A program for the automatic bifurcation analysis of autonomous systems. *Congr. Numer* **30**, 265–284 (1981).
16. Farrell, P.E., Beentjes, C.H.L., Birkisson, A.: The computation of disconnected bifurcation diagrams. [arXiv:1603.00809](https://arxiv.org/abs/1603.00809) (2016).

17. Fre, S., Huyghe, M., Mourikis, P., Robine, S., Louvard, D., Artavanis-Tsakonas, S.: Notch signals control the fate of immature progenitor cells in the intestine. *Nature* **435**(7044), 964–968 (2005).
18. Gelfand, I.M., Kapranov, M.M., Zelevinsky, A.V.: *Discriminants, resultants, and multidimensional determinants*. Mathematics: Theory & Applications, Birkhäuser Boston, Inc., Boston, MA (1994).
19. Glassner, A.S. (ed.): *An Introduction to Ray Tracing*. Academic Press Ltd., London, UK (1989).
20. Glendinning, P.: *Stability, instability and chaos: an introduction to the theory of nonlinear differential equations*. Cambridge Texts in Applied Mathematics, Cambridge University Press, Cambridge (1994).
21. Golubitsky, M., Schaeffer, D.G.: *Singularities and groups in bifurcation theory*. Vol. I, Applied Mathematical Sciences, vol. 51. Springer-Verlag, New York (1985).
22. Golubitsky, M., Stewart, I.: *Singularities and groups in bifurcation theory*, vol. 1. Springer Science & Business Media (1985)
23. Griffin, Z.A., Hauenstein, J.D.: Real solutions to systems of polynomial equations and parameter continuation. *Adv. Geom.* **15**(2), 173–187 (2015).
24. Gross, E., Harrington, H.A., Rosen, Z., Sturfels, B.: Algebraic systems biology: A case study for the wnt pathway. *Bulletin of Mathematical Biology* **78**(1), 21–51 (2016)
25. Grün, D., Lyubimova, A., Kester, L., Wiebrands, K., Basak, O., Sasaki, N., Clevers, H., van Oudenaarden, A.: Single-cell messenger RNA sequencing reveals rare intestinal cell types. *Nature* **525**(7568), 251–255 (2015)
26. Hanan, W., Mehta, D., Moroz, G., Pouryahya, S.: Stability and bifurcation analysis of coupled Fitzhugh-Nagumo oscillators. "Extended abstract" published in the Joint Conference of ASCM2009 and MACIS2009, Japan, 2009. arXiv:1001.5420 (2010)
27. Hao, W., Hauenstein, J.D., Hu, B., Sommese, A.J.: A three-dimensional steady-state tumor system. *Appl. Math. Comput.* **218**(6), 2661–2669 (2011).
28. Hauenstein, J.D., Sommese, A.J.: Witness sets of projections. *Appl. Math. Comput.* **217**(7), 3349–3354 (2010).
29. Hauenstein, J.D., Sottile, F.: Algorithm 921: alphaCertified: Certifying solutions to polynomial systems. *ACM Trans. Math. Softw.* **38**(4), 28 (2012).
30. Hauenstein, J.D., Wampler, C.W.: Isosingular sets and deflation. *Foundations of Computational Mathematics* **13**(3), 371–403 (2013).
31. Hernandez-Vargas, E.A., Mehta, D., Middleton, R.H.: Towards modeling HIV long term behavior. *IFAC Proceedings Volumes* **44**(1), 581–586 (2011).
32. Lazard, D., Rouillier, F.: Solving parametric polynomial systems. *Journal of Symbolic Computation* **42**(6), 636–667 (2007).
33. Lu, Y., Bates, D.J., Sommese, A.J., Wampler, C.W.: Finding all real points of a complex curve. In: *Algebra, geometry and their interactions*, *Contemp. Math.*, vol. 448, pp. 183–205. Amer. Math. Soc., Providence, RI (2007).
34. Montaldi, J.: The path formulation of bifurcation theory. In: *Dynamics, Bifurcation and Symmetry* (Cargèse, 1993), *NATO Adv. Sci. Inst. Ser. C Math. Phys. Sci.*, vol. 437, pp. 259–278. Kluwer Acad. Publ., Dordrecht (1994).
35. Niu, W., Wang, D.: Algebraic approaches to stability analysis of biological systems. *Mathematics in Computer Science* **1**(3), 507–539 (2008).
36. Pettigrew, D.B., Smolen, P., Baxter, D.A., Byrne, J.H.: Dynamic properties of regulatory motifs associated with induction of three temporal domains of memory in aplysia. *J. Comput. Neuro.* **18**(2), 163–181 (2005).

37. Piret, K., Verschelde, J.: Sweeping algebraic curves for singular solutions. *J. Comput. Appl. Math.* **234**(4), 1228–1237 (2010).
38. Simon, P.L., Farkas, H., Wittmann, M.: Constructing global bifurcation diagrams by the parametric representation method. *J. Comput. Appl. Math.*, **108**(1-2), 157–176 (1999).
39. Sommese, A.J., Wampler, II, C.W.: *The numerical solution of systems of polynomials arising in engineering and science*. World Scientific Publishing Co. Pte. Ltd., Hackensack, NJ (2005).
40. Song, H., Smolen, P., Av-Ron, E., Baxter, D.A., Byrne, J.H.: Bifurcation and singularity analysis of a molecular network for the induction of long-term memory. *Biophysical journal* **90**(7), 2309–2325 (2006).
41. Sprinzak, D., Lakhanpal, A., Lebon, L., Santat, L.A., Fontes, M.E., Anderson, G.A., Garcia-Ojalvo, J., Elowitz, M.B.: Cis-interactions between Notch and Delta generate mutually exclusive signalling states. *Nature* **465**(7294), 86–90 (2010).
42. Sturmfels, B.: *Solving systems of polynomial equations*, CBMS Regional Conference Series in Mathematics, vol. 97. Published for the Conference Board of the Mathematical Sciences, Washington, DC; by the American Mathematical Society, Providence, RI (2002).
43. Verschelde, J.: Algorithm 795: PHCpack: A general-purpose solver for polynomial systems by homotopy continuation. *ACM Transactions on Mathematical Software (TOMS)* **25**(2), 251–276 (1999).
44. Visvader, J.E., Clevers, H.: Tissue-specific designs of stem cell hierarchies. *Nat Cell Biol* **18**(4), 349–355 (2016).
45. Wampler, C., Sommese, A., Morgan, A.: Numerical continuation methods for solving polynomial systems arising in kinematics. *Journal of mechanical design* **112**(1), 59–68 (1990).
46. Xia, B.: Discoverer: a tool for solving semi-algebraic systems. *ACM Communications in Computer Algebra* **41**(3), 102–103 (2007).
47. Yeung, T.M., Chia, L.A., Kosinski, C.M., Kuo, C.J.: Regulation of self-renewal and differentiation by the intestinal stem cell niche. *Cellular and Molecular Life Sciences* **68**(15), 2513–2523 (2011).